Chapter 6

Field Emission

6.1 Introduction

Electron beams play a central role in many applications and basic research tools. For example, electron emission is used in cathode ray tubes, x-ray tubes, scanning electron microscopes, and transmission electron microscopes. In many of these applications, it is desirable to obtain a high density of narrow electron beams, with each beam tightly distributed in energy. So-called electron guns, which operate on thermionic emission of electrons from hot cathodes, are extensively utilized for this purpose. However, achieving electron beams with narrow energy distributions is difficult because of thermal broadening of the emitted electrons. Thus, field emission from cold cathodes is of much interest, but requires large electric fields that cause migration of atoms at the tip surface, making it difficult to achieve stable operation over long periods of time. Carbon nanotubes may offer a solution to these issues. Indeed, carbon nanotubes have many advantages for cold field emission: the inertness and stability of nanotube tips to long periods of operation compared to metal and diamond tips; low threshold voltage for cold field emission; low temperature of operation; fast response times; low power; and small size. As will be discussed later in this chapter, prototype devices using the superior field emission properties of nanotubes have already been demonstrated. These devices include x-ray tubes [Sug01], scanning x-ray sources [Zha05], flat panel displays [Cho99b], and lamps [Cro04].

Before going into the details of field emission, we begin by introducing the early experimental work that established the promise of carbon nanotubes for field emission [Hee95]. Figure 6.1 shows the experimental set-up to measure the field emission from carbon nanotube films. There, a film of carbon nanotubes, with the nanotubes oriented perpendicular to the substrate serves as the electron emitter. A copper grid sits 20 microns above the nanotube film, with the separation provided by a mica sheet. Application of a voltage between the copper grid and the nanotube film creates a beam of electrons that passes through the copper grid and is detected at an electrode 1 cm away from the copper grid. (It should be noted that these experiments are performed under high vacuum where the field emitter device sits in a vacuum chamber with a residual pressure of 10^{-6} torr.) A current versus voltage curve for such a device is shown in Figure 6.1, indicating a large increase of the current in the forward bias direction (the emission is diode-like: for negative voltages, very little current flows). To verify that the beam indeed consists of electrons, the beam was deflected in a magnetic field, and the deflection corresponds to that of particles with the free electron mass. The inset in this figure shows a plot of $\log\left(I/V^2\right)$ vs V^{-1}, the so-called Fowler-Nordheim plot (more will be said about Fowler-Nordheim emission below). Importantly, it is found that the field enhancement factor is about 100 times larger than conventional field emitter tips. To further establish the promise of carbon nanotubes for field emission, the stability of the

field emitters was studied as a function of time (Figure 6.1). Current fluctuations were observed to be less than 10%, which is remarkable considering that the current depends exponentially on the voltage. Little degradation was observed, even after operation periods as long as 48 hours.

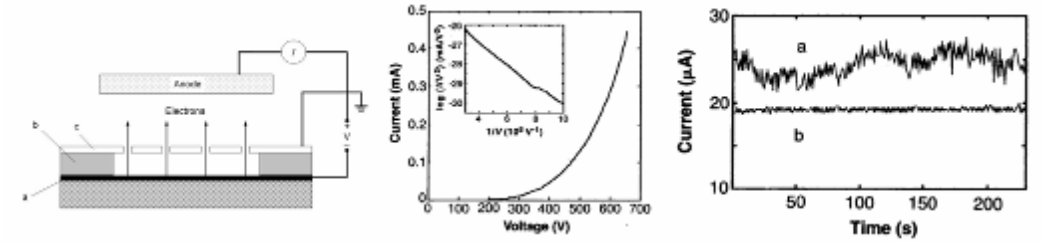

Figure 6.1: The left panel shows a sketch of a field emission electron source. The emitter is a film of aligned carbon nanotubes (a), with the nanotubes aligned perpendicular to a polytetrafluoroethylene substrate. The nanotubes have average diameters of 10 nm and are about 1 micron long. A sheet of mica (b) with a hole of 1 mm diameter is bonded to the nanotube film. The hole is covered with an electron microscopy copper grid (c), which is used to apply the emission voltage. The current is measured at a collector electrode 1 cm away from the grid. The middle panel shows the current versus field emission voltage, with the Fowler-Nordheim plot in the inset. The right panel shows the emitted current as a function of time. The bare fluctuations are on the order of 10% (curve a) but can be reduced to 2% with a feedback system (curve b). *Middle and right figures from Ref. [Hee95].*

The theory of field-emission was originally developed by Fowler and Nordheim [Fow28], and has since been refined to include effects such as details of the tunneling potential and material-specific density of states. However, the basic aspects of field emission can be captured from a simple theory of tunneling across a triangular potential barrier using the WKB approximation (Fowler and Nordheim used a more accurate approach where the wavefunctions are matched at appropriate boundaries). We present the simplified theory here as it serves to illustrate the basic physics behind field-emission, and in any case recovers the general behavior.

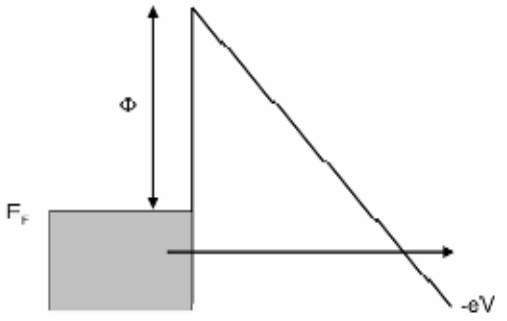

Figure 6.2: Illustration of potential profile for field-emission from a metal. Φ is the metal workfunction, V is the applied potential between the anode and the cathode, and E_F is the metal Fermi level. Electrons in the filled states below E_F (grey shading) tunnel across the triangular potential energy barrier to the anode.

Figure 6.2 illustrates the situation for field emission from a metallic surface. In the metal (cathode), electronic states are filled up to the Fermi level. Upon application of a voltage to the anode, a linear potential drop occurs across the vacuum gap, leading to a triangular potential energy barrier of height Φ equal to the metal workfunction. Electrons below the Fermi level tunnel through the triangular barrier (at finite temperature, there is a distribution of electrons above the Fermi level; here we consider the zero temperature limit since it illustrates the main points of the theory.) The current density is of the form

$$J = e\int dE_x d\vec{k}_\perp v_x(E_x) D(E_x,\vec{k}_\perp) T(E_x,\vec{k}_\perp) f\left(E_x,\vec{k}_\perp\right) \tag{2.1}$$

where $D(E_x,\vec{k}_\perp)$ is the density of electronic states in the metal, $v_x(E_x)$ is the electron velocity in the *x* direction, $T(E_x,\vec{k}_\perp)$ is the transmission probability across the tunnel barrier, and $f\left(E_x,\vec{k}_\perp\right)$ is the fermi function. Here, E is the total energy of the electron, E_x is the energy in the *x* direction and $\vec{k}_\perp$ is the momentum vector perpendicular to the tunneling direction. For a free electron gas we have the relationships

$$\begin{aligned} E_x &= E - \frac{\hbar^2 k_\perp^2}{2m} \\ E_x &= \frac{\hbar^2 k_x^2}{2m} \end{aligned} \tag{2.2}$$

and the velocity is

$$v_x = \frac{1}{\hbar}\frac{\partial E}{\partial k_x} = \frac{1}{m}\sqrt{\frac{2mE_x}{\hbar^2}}. \tag{2.3}$$

The tunneling probability across the barrier is obtained using the WKB approximation:

$$T(E) = \exp\left[-2\int_{x_1=0}^{x_2(E)} k(x,E)dx\right] \tag{2.4}$$

where x_1 and x_2 are the classical turning points. For a free electron in a potential $V(x) = \Phi - eV\frac{x}{L}$ we have

$$T(E_x) = \exp\left[-2\sqrt{\frac{2m}{\hbar^2}}\int_{x_1=0}^{x_2(E_x)} \sqrt{\Phi - eV\frac{x}{L} - E_x}\,dx\right]. \tag{2.5}$$

Integration of this equation with $x_2(E_x) = L\left(\Phi - E_x\right)/eV$ gives

$$T(E_x) = \exp\left[-\frac{4}{3}\sqrt{\frac{2m}{\hbar^2}}\frac{L}{eV}\left(\Phi - E_x\right)^{3/2}\right] \approx \exp\left[-\frac{4}{3}\sqrt{\frac{2m}{\hbar^2}}\frac{L}{eV}\Phi^{3/2} + 2\sqrt{\frac{2m}{\hbar^2}}\frac{L}{eV}\Phi^{1/2}E_x\right]. \tag{2.6}$$

A Taylor expansion around the Fermi level was used to obtain the last approximation, since the tunneling probability decreases rapidly below the Fermi level. The total current is then given by

$$J = e\int dE_x v_x(E_x)T(E_x)\int D(E_x,\vec{k}_\perp)f\left(E_x,\vec{k}_\perp\right)d\vec{k}_\perp. \tag{2.7}$$

For the free electron gas, the last integral at zero temperature is

$$\int D(E_x,\vec{k}_\perp)f\left(E_x,\vec{k}_\perp\right)d\vec{k}_\perp = \frac{2\pi}{\partial E/\partial k_x}\int_0^{\sqrt{\frac{2mE_x}{\hbar^2}}} k_\perp dk_\perp = \frac{\pi m}{\hbar}\sqrt{\frac{2mE_x}{\hbar^2}}. \tag{2.8}$$

The current density is then

$$J = e\frac{2\pi m}{\hbar^3}\exp\left(-\frac{4}{3}\sqrt{\frac{2m}{\hbar^2}}\frac{L}{eV}\Phi^{3/2}\right)\int_{-\infty}^{0} dE_x E_x \exp\left(2\sqrt{\frac{2m}{\hbar^2}}\frac{L}{eV}\Phi^{1/2}E_x\right) \tag{2.9}$$

with the final result

$$J = \frac{e^3V^2}{4L^2\hbar\Phi}e^{-\frac{4}{3}\sqrt{\frac{2m}{\hbar^2}}\frac{L}{eV}\Phi^{3/2}}. \tag{2.10}$$

It is useful to recap the factors that lead to Equation (6.10):

1. *Tunneling is through a triangular barrier.* The actual shape of the barrier differs from a triangular barrier for many reasons, including the presence of image potentials and the shape of the emitter. As we will see below, this is particularly important for carbon nanotubes because of the small dimensions and high aspect ratio.
2. *The emitter is modeled as a free electron gas.* This obviously neglects the bandstructure of the emitter, and quantitative comparison with experiments requires the inclusion of these effects. For carbon nanotubes, the electronic structure at the tip is important in determining the field emission properties.
3. *The tunneling barrier height is independent of the applied voltage.* The derivation above assumed that the tunneling barrier height is equal to the metal workfunction, for any applied voltage. In carbon nanotubes, the barrier height can change by as much as 0.15 eV/(Vμm^{-1}).

Some of these effects are encountered in traditional materials as well, and usually the Fowler-Nordheim model for field-emission is generally written as

$$I = aV^2 \exp\left(-\frac{b\Phi^{3/2}}{\beta V}\right) \tag{2.11}$$

where β is the so-called field-enhancement factor according to the relation $F = \beta V / L$ where F is the electric field. This important parameter, which depends on the geometry of the field-emission tip, represents the fact that the electric field at the tip can be enhanced from the triangular profile value. In general, large values of β are desirable since it implies that the electric field near the tip is large, and hence electrons can more easily tunnel from the field emission tip. A consequence is that lower threshold voltages are required for field-emission; nanotubes, with their high aspect ratio are thus particularly attractive for this reason.

As the discussion of the basic Fowler-Nordheim field emission theory above has indicated, an important question is the validity of the traditional Fowler-Nordheim model to describe field emission from nanotube tips. The unique band structure with van hove singularities in the density of states and localized/quasi-localized states at the tip may necessitate the need for a new model to describe field emission from nanotubes. While both experiments and theory have explored this topic, there is no clear conclusion. However, most experiments show that the *total* field emission current as a function of bias is quite consistent with the Fowler-Nordheim model in single wall nanotubes [Rin95, Jon04a], ropes [Lov00, Bon02], films [Bon02, Che95, Hee95] and patterned films [Wan98]. A field emission tip consisting of a single multiwall nanotube with a radius of 5 nm, attached to a tungsten tip is shown in Figure 6.3a [Jon04a]. Here, one can clearly see the large aspect ratio (length to diameter) achieved experimentally. The current-voltage characteristics are reasonably consistent with the Fowler-Nordheim model over a current window spanning more than two orders of magnitude (Figure 6.3b). Deviations from the Fowler-Nordheim model for total current have been observed in specific samples because of adsorbates and possibly quantized energy levels in the tip. These topics will be discussed in more detail below.

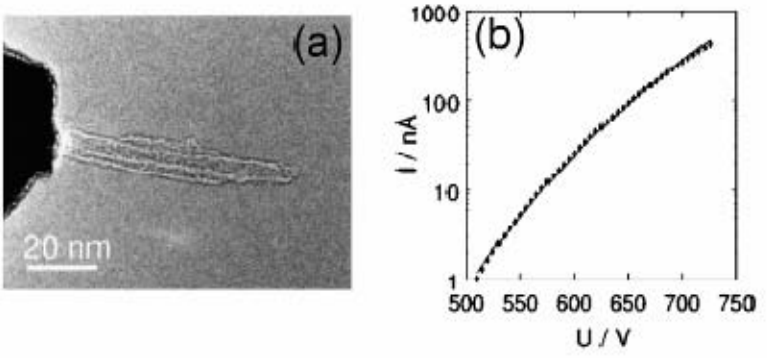

Figure 6.3: (a) Transmission electron microscope image of a nanotube on a tungsten tip. (b) Field emission current as a function of applied bias. Note the good match to the Fowler-Nordheim model Equation (6.11) (solid line). *Figure from Ref. [Jon04a].*

While the total current can show good agreement with the Fowler-Nordheim model, the total energy distribution of electrons is a more sentitive probe of the electronic structure

of the nanotube tip. Experiments and modeling show that the total energy distribution (TED) of the field-emitted current can differ from the Fowler-Nordheim behavior. While experiments on a single nanotube showed reasonable agreement with the Fowler-Nordheim model [Jon05], experiments have shown deviations in the total energy distribution in samples consisting of a bundle of single wall nanotubes [Lov00]. Modeling [Car97, Vit99, Ade00] has shown that localized states in the tip cause a significant change in the density of states and the emitted current contains signatures of these states.

The total energy distribution corresponding to the experiment discussed in Figure 6.3 is shown in Figure 6.4a. The TED reasonably follows the Fowler-Nordheim model over a large energy window. In contrast, field emission from a single wall nanotube bundle shows a total energy distribution that is different from the Fowler-Nordheim model, as compared in panel (b) of the same figure [Lov00]. While the net current agrees with the Fowler-Nordheim model, noticeable deviations are seen in the total energy distribution around the Fermi energy and at energies -0.6 eV and -1.05 eV below the Fermi energy. The deviations around the Fermi energy is attributed to dangling bond states in open nanotubes [Vit99], while the deviations at the other two energies are found to correlate with van Hove singularities in the nanotube density of states.

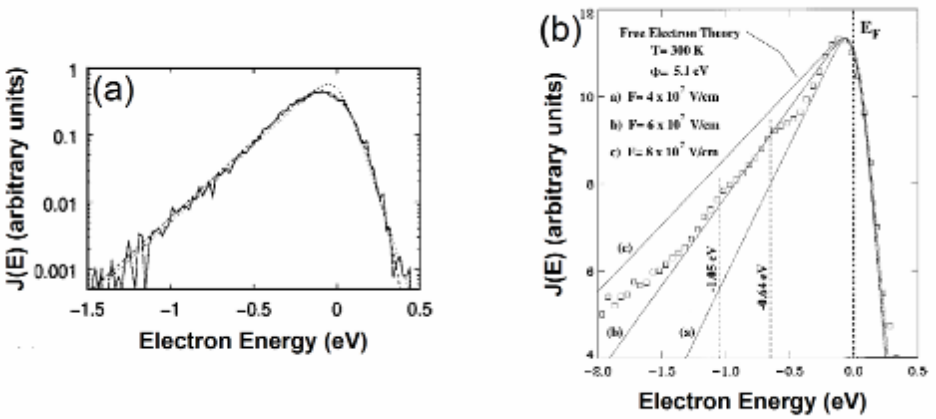

Figure 6.4: (a) Total energy distribution of emitted current corresponding to the single nanotube in Figure 6.3, at room temperature, applied voltage of 552.8 V, and an emitted current of 11 nA. *Figure from Ref. [Jon05].* (b) Log of total energy distribution versus energy for electrons field emitted from a single-wall carbon nanotube rope. The solid lines show the predictions of the Fowler-Nordheim model for three different values of the electric field *F*. The Fermi energy (E_F) and features representing deviations from the Fowler-Nordheim model at energies of -0.64 and -1.05 eV are marked by dotted lines. *Figure from Ref. [Lov00].*

To gain more insight into the factors that influence field emission from carbon nanotubes, detailed calculations of the properties of field enhancement, potential barriers, and the role of nanotube electronic structure have been performed [Bul03, Zhe04]. Figure 6.5 shows the electric field lines and electric field intensity near the tip of a (5,5) carbon

nantube, obtained by solving Laplace's equation in the presence of the metallic nanotube. The calculations indicate that the electric field is dramatically enhanced near the tip.

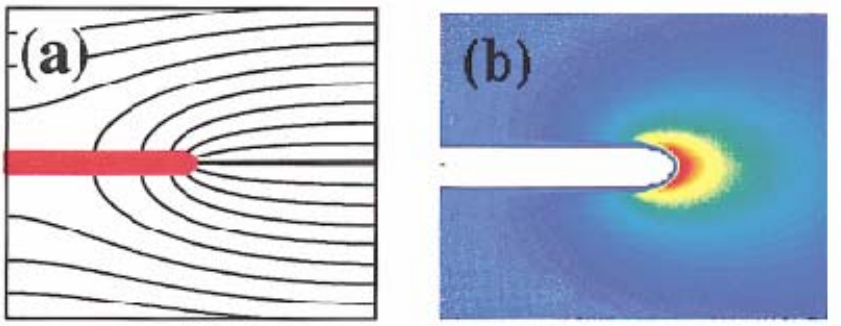

Figure 6.5: Calculated electric field lines and field intentity near the tip of a carbon nanotube. (a) Electric field lines near the tip of a (5,5) nanotube. (b) Field intensity near the tip of a (10,10) nanotube, showing the field enhancement near the tip. *Figure from Ref. [Bul03].*

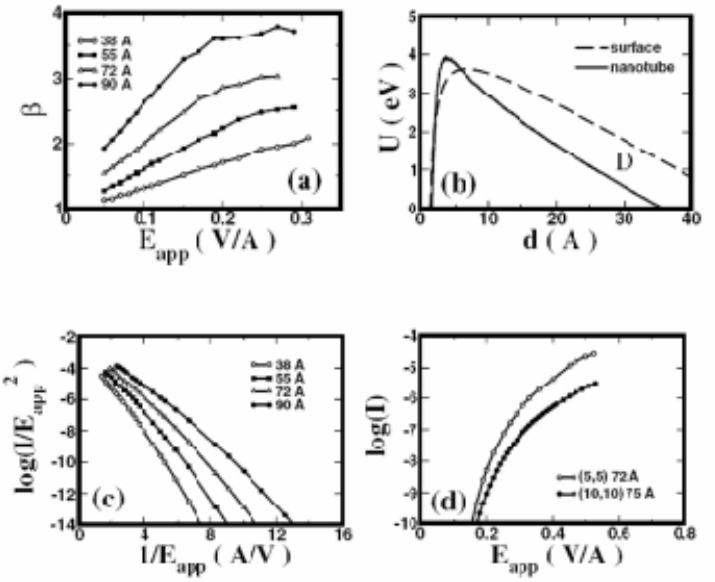

Figure 6.6: Calculated properties of field emission from nanotube tips. Panel (a) shows the field enhancement factor β as a function of the applied field and nanotube length. In (b) the calculated shape of the tunneling barrier for a (5,5) nanotube is compared with that of a planar metallic surface. (c) Fowler-Nordheim plots for (5,5) nanotubes of different lengths. (d) Current versus applied field for (5,5) and (10,10) nanotubes of roughly the same length. *Figure from Ref. [Bul03].*

What is perhaps more important is that the field enhancement factor β is found to be strongly dependent on the applied field, as shown in Figure 6.6a. One consequence of this effect is that the potential energy barrier through which the electrons must tunnel is dependent on the electric field, and deviates from that of a planar surface (Figure 6.6b). Because of these effects, the current deviates from the traditional Fowler-Nordheim behavior, and a plot of $\log\left(I/V^2\right)$ vs V^{-1} deviates from a straigth line (Figure 6.6c).

Modeling also provides some detailed information about field emission from individual atomic sites at carbon nanotube tips. In Figure 6.7, the intentity of electron emission is shown for the atoms at the nanotube tip, as the electric field is increased. Initially, atoms forming a pentagonal ring at the apex start emitting; as the field is increased, more and more atoms contribute to the field emission current. It is interesting to note that there are five other pentagonal rings in the cap of the nanotube, and because these have larger local density of states, it could be expected that they would contribute a significant fraction of the field emission current. While these sites are indeed found to give large field emission at the higher fields (Figure 6.7d), many other atomic sites also contribute to the emission.

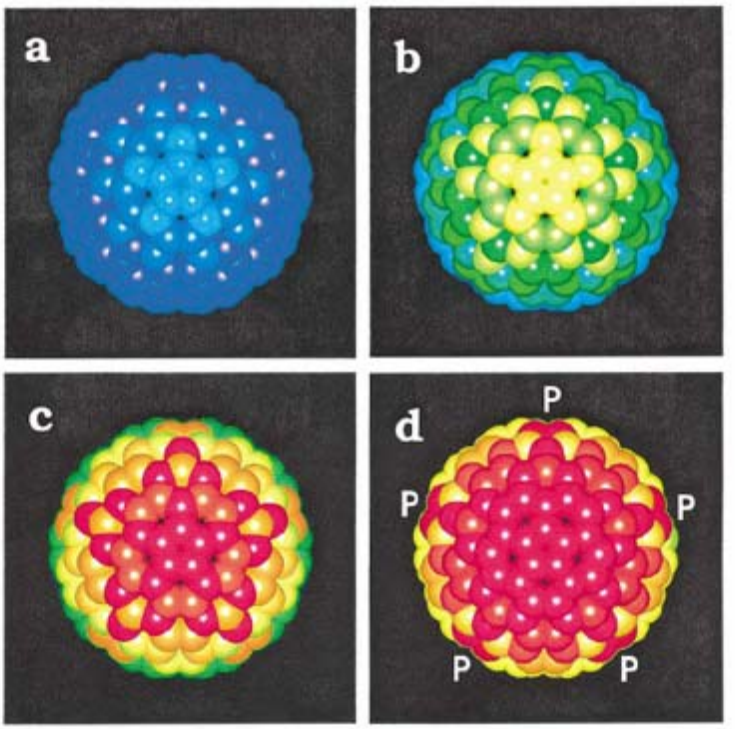

Figure 6.7: Color plots of electron emission from the tip of a (10,10) nanotube (violet = low emission intensity, red = high emission intensity). The electric field increases from panel (a) to (d) with values of 0.2, 0.3, 0.4 and 0.45 V/A. At low fields, only atoms near the apex of the cap emit; as the field is increased, more and more atoms begin to emit. *Figure from [Bul03].*

A limitation of the above calculations is that only the cap the carbon nanotube is considered. However, as the results of Figure 6.6 indicate, the behavior of the nanotube emission depends on the length of the nanotube. Thus, to make contact with experiments that utilize nanotubes of micron-size length, it is necessary to extend the calculations to much longer nanotubes, while still maintaining an atomistic description of the tip region. Such calculations have been performed [Zhe04] by utilizing a hybrid quantum mechanics and molecular mechanics approach, where 8000 atoms near the tip are simulated

quantum mechanically, while the rest are treated as electrostatic point charges. This allows for the simulation of a 1 micron-long carbon nanotube in a field emission geometry, as shown in Figure 6.8. In such a calculation, the induced charge on the nanotube near the tip is obtained by the quantum mechanical calculation, while the charge in the section treated by molecular mechanics is obtained as follows: For a metallic carbon nanotube, the density of states is constant around the Fermi level, and a deviation of the electrostatic potential $\delta V(z)$ will induce a charge $\rho(z) \propto \delta V(z)$. Thus, the Poisson equation will be of the form $\nabla^2 \delta V(z) \propto \rho(z)$ or $\nabla^2 \rho(z) \propto \rho(z)$ and the induced charge is of the form

$$\rho(z) \sim \rho(L') \exp\left[-\left(L'-z\right)/\lambda\right] \tag{2.12}$$

where λ is the decay length and $\rho\left(L'\right)$ is the induced charge at the interface between the quantum mechanical and molecular mechanics regions. The boundary condition on the cathode is satisfied by considering image charges, as shown in Figure 6.8.

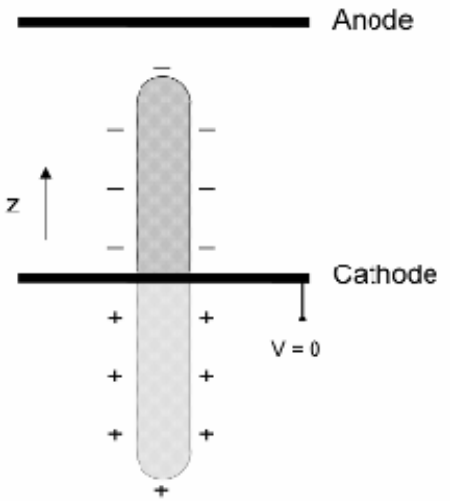

Figure 6.8: Sketch of the system used for calculating the field emission properties of micrometer long carbon nanotubes. *After Ref. [Zhe04].*

Results of such calculations are shown in Figure 6.9. First, the induced charge is found to be only a few percent of the total charge at the tip, and is found to oscillate along the length of the nanotube. Most importantly, the induced charge is found to be concentrated near the tip, with a decay length of about 0.5 μm (inset Figure 6.9c), indicating that simulation of the entire length of the nanotube is necessary to capture all of the electronic charge contributions.

Perhaps the most surprising result from these calculations is that the electric field is found to penetrate the nanotube near the tip region, as shown in Figure 6.10a. Because of this effect, the field enhancement factor is found to be as much as a factor of three larger than what would be predicted without field penetration. Panel (b) in this figure shows a close-

up of the electrostatic potential near the tip, with points marking the Fermi level (-4.5 eV). The Fermi level is below the potential barrier, indicating that the electrons have to tunnel through a barrier. It is also found that the barriers are thicker and higher on the side of the nanotube, indicating that preferential emission from the tip is expected. A closer look at the potential energy profile near the nanotube tip shows that the barrier height depends significantly on the applied field. Indeed, it is found that the barrier height is reduced from 4.5 eV to 2 eV under a field of 14 V μm^{-1}.

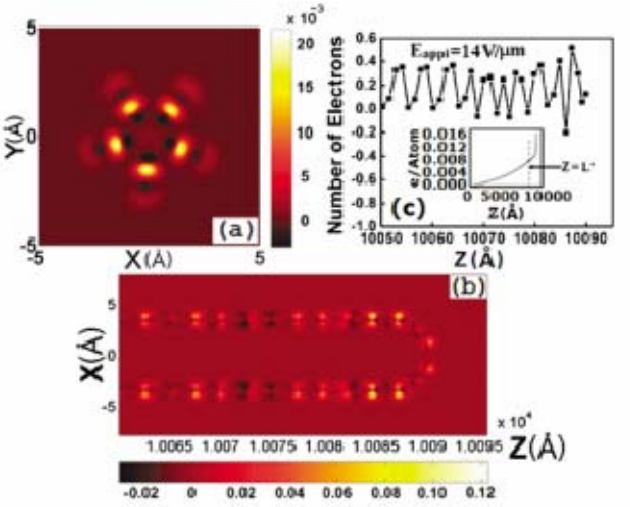

Figure 6.9: (a) Induced charge distribution at the top layer of the nanotube cap. (b) Induced charge distribution in a plane bisecting the nanotube. (c) Number of induced electrons on each layer near the tip region. Excess charge along the entire nanotube is plotted in the inset. *Figure from Ref. [Zhe04].*

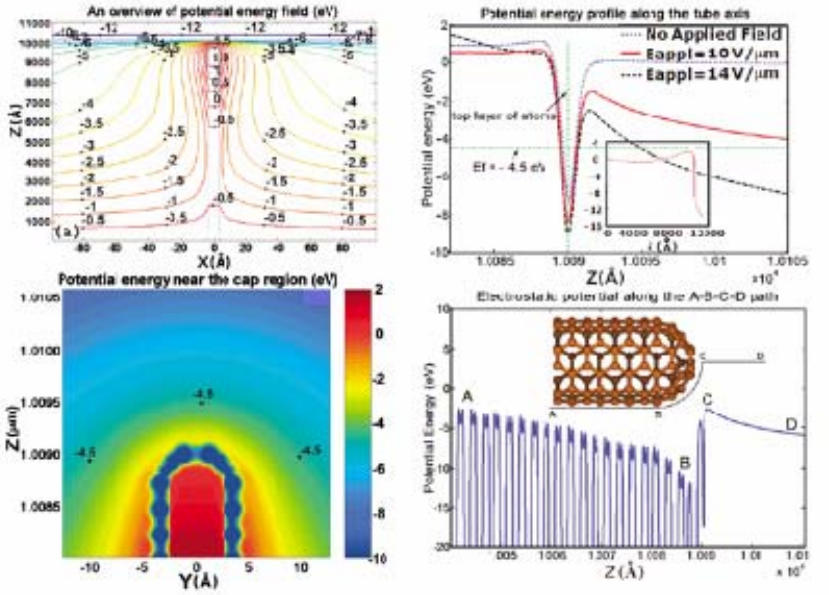

Figure 6.10: Left: Potential energy contour plots for a (5,5) nanotube for a field of 14 V μm^{-1}. The axis of the nanotube is at x=0. Right: Potential energy profiles near the nanotube cap. *Figures from Ref. [Zhe04].*

The predictions of localized electrical fields at the tip of carbon nanotubes during field-emission have been verified using electron holography experiments [Cum02]. In this technique, illustrated in Figure 6.11, a multiwall carbon nanotube is positioned 6 μm away from a gold electrode, and a high bias voltage is applied between the two to induce field emission. An electron beam perpendicular to the field-emitted electron beam comes from a transmission electron microscope, and is split by a biprism after traversing the nanotube region; the two halves of the beam converge onto an image plane where the hologram is recorded. Interference fringes provide information on the relative phase between the two halves of the beam, which is related to the local electrostatic potentials that the beam traverses. The phase shift acquired by the electrons as they traverse a spatially–dependent potential V is given by the expression

$$\Delta\phi = \alpha \int_{\text{beam path}} V dl \qquad (2.13)$$

where the integral is over the path traversed by the electron beam and α is a parameter that depends on details of the transmission electron microscope.

Figure 6.11 shows an electron hologram image taken from a single carbon nanotube during field emission. The main diffraction pattern comes from the biprism and is not related to the phase change; a more detailed view of the region around the nanotube shows that additional finges are present with periodicity of about 4 nm, and these carry the information about the electric fields around the nanotube tip. When the phase difference is extracted from these images, one can clearly see the carbon nanotube in the

phase image (see middle panel of Figure 6.11, taken at zero bias voltage), indicating that the electron beam is going through a difference of integrated potential when passing through the nanotube. In the presence of an applied bias between the nanotube and the gold electrode, a spatially-varying potential is created, causing a spatially-dependent phase shift, as shown in the middle panels of Figure 6.11 for 70 V and 120 V. In these images, stripes are observed because the phase shift is plotted as modulo 2π; from these, the phase gradient can be calculated and provides smooth images of the electric field in the nanotube region. These phase gradient images clearly indicate that electric fields are concentrated near the tip of the nanotube and not at nanotube defects on the sidewall.

These experiments also provide evidence that current fluctuations during field emission are not caused by large changes in the electric field distribution around the nanotube, but are most probably due to small fluctuations of the local electronic structure, as can arise due to adsorbates. During the electron holography experiments, the field emission current is observed to fluctuate by as much as 80%, but the electron hologram fringe patterns are observed to remain sharp—over the acquisition time of several seconds, these patterns would appear blurry even for small fluctuations of the electric field. Thus, the fluctuations in the electric field amount to only a few percent, much too small to explain the fluctuations in the field-emitted current.

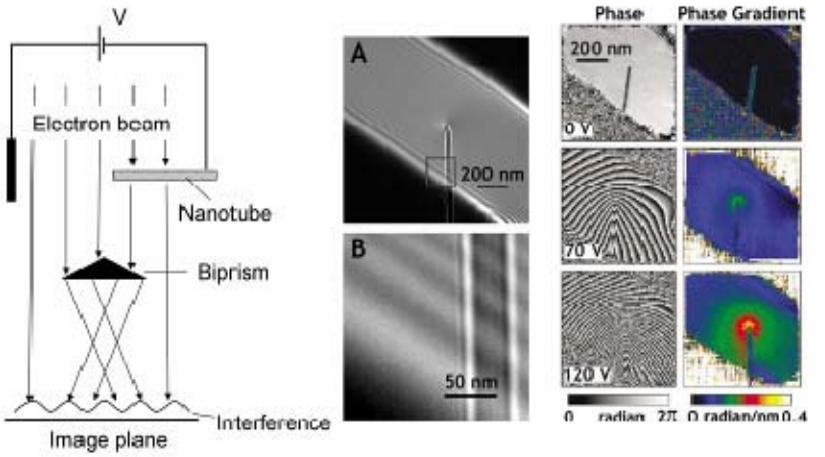

Figure 6.11: Left panel: Schematic of electron holography experiment on a field-emitting carbon nanotube. Middle panel: Electron hologram of a carbon nanotube biased during field-emission at 120 V (A) and a more detailed view of the boxed area (B). Right panel: Phase shift and phase gradient from electron hologram experiments at bias voltages of 0, 70 and 120 V. *Middle and right figures from Ref. [Cum02].*

A measure often used to quantify the quality of emission sources is the reduced brightness B_r defined as

$$B_r = \frac{dI}{d\Omega}\frac{1}{V}\frac{1}{\pi r_v^2} \tag{2.14}$$

where I is the emission current, Ω is the solid angle, V the acceleration voltage and r_v the virtual source size. The virtual source size is the area at the tip from which the emission appears to originate when the trajectories of electrons are traced back [Jon04b]; its value can be obtained by measuring the diffraction pattern caused when the electron beam impinges on a sharp edge, as illustrated in Figure 6.12. In such an experiment, a diffraction pattern consisting of several maxima is observed at a distance z_2 from the sharp edge. Quantitatively, the position of the maxima is given by the expression

$$x(N) - x(0) = z_2\sqrt{\frac{2\lambda}{z_1}}\left(\sqrt{n+\frac{3}{8}} - \sqrt{\frac{3}{8}}\right) \tag{2.15}$$

where

$$x(0) = z_2\sqrt{\frac{2\lambda}{z_1}}\frac{3}{8} \tag{2.16}$$

is the position of the first maximum and λ is the electron wavelength. The virtual source size can be obtained from these expressions [Jon02] as

$$r_v = \frac{\lambda z_2}{\pi x(N)}. \tag{2.17}$$

Figure 6.12 shows multi-wall carbon nanotube attached to a tungsten tip and the resulting Fresnel oscillations measured due to electron emission from this source near a sharp edge. As shown in the inset of the right panel, up to eight maxima are visible, so that counting from zero we have $x(N) = x(7) = 4.0$ mm; with the value $z_2 = 16$ cm this gives a virtual source size $r_v = 2.1$ nm. This value is somewhat less than the 2.7 nm radius of curvature of this particular carbon nanotube.

To obtain the reduced brightness, the value of $dI/d\Omega = 16\ \mu\text{Asr}^{-1}$ was measured using a Faraday cup for a similar carbon nanotube of $r_v = 2.5$ nm and an acceleration voltage $V = 319$ V ; this gives a reduced brightness $B_r \sim 3\times10^9$ A sr^{-1} m^{-2} V^{-1}. This value can be compared [Jon02] with that of traditional Schottky emitters of cold field-emission guns, which have reduced brighness values less than 2×10^8 A sr^{-1} m^{-2} V^{-1}. The nanotube emitter therefore has a reduced brightness at least an order of magnitude larger than these conventional sources.

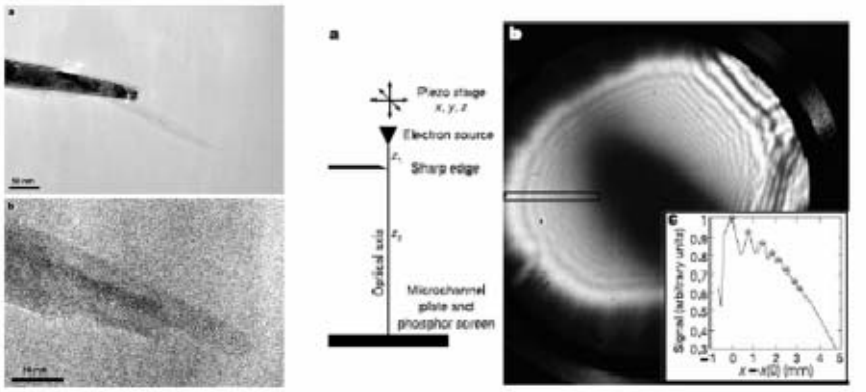

Figure 6.12: (Left) Transmission electron microscopy images of a multiwall carbon nanotube at the end of a tungsten tip. Experrimental set-up to measure the virtual source size of the carbon nanotube emitter. The carbon nanotube is positioned close to a sharp edge, causing a Fresnel diffraction pattern on a screen. (b) The interference pattern from the nanotube on the left, including a line scan (averaged over the rectangle in the main panel) showing the first few maxima. *Figure from Ref. [Jon02].*

6.2 Adsorbates

Experiments have shown a significant deviation from the Fowler-Nordheim model in the presence of adsorbates. Adsorbates can have many effects, such as changing the work function for emission, the width of the tunneling barrier or the density of electronic states. Furthermore, because large electric fields are applied to the tips during field emission, adsorbates can change their location on the surface or even desorb. These effects can lead to unusual features in the field-emitted current. To probe these effects, controlled experiments have been performed [Dea00], where the field emission properties of clean single wall carbon nanotubes is compared to the field emission in the presence of intentionally introduced adsorbates. These adsorbates are introduced by exposing the nanotube tip to H_20 under a partial pressure of 10^{-7} Torr for five minutes. As can be seen in Figure 6.13 there is a qualitative difference between the field emission of the clean and adsorbate-covered nanotube tips. For clean nanotubes, the *I-V* curve follows the Fowler-Nordheim model; in contrast, the field emission in the presence of adsorbates shows an enhanced current at the lower voltages, followed by a partial saturation and finally a current increase at higher voltages that follows the clean nanotube emission. A downward sweep after such large applied voltages shows current-voltage characteristics of a clean sample. Heating the tip to 900 K under field emission conditions leads to regular field emission behavior without current saturation because of adsorbate desorbtion. These observations are explained by the adsorbate-induced increase in the field emission current at the lower voltages. At intermediate voltages, the adsorbates are displaced into configurations that decrease the tunneling current. Finally, at high enough voltages, the adsorbates desorb from the nanotube tip—the high current behavior and the

downward sweep thus follow that of the clean nanotube. This remarkable experiment also showed that adsorbates change the shape of the field emission pattern (Figure 6.13b). The field emission pattern in a clean sample is shown in panel (i). Introducing water causes a significant deviation in the pattern as shown in panel (ii). The reverse sweep after applying a voltage of 2300 V matches the pattern with a clean tip due to desorbtion of adsorbate as shown in panel (iii).

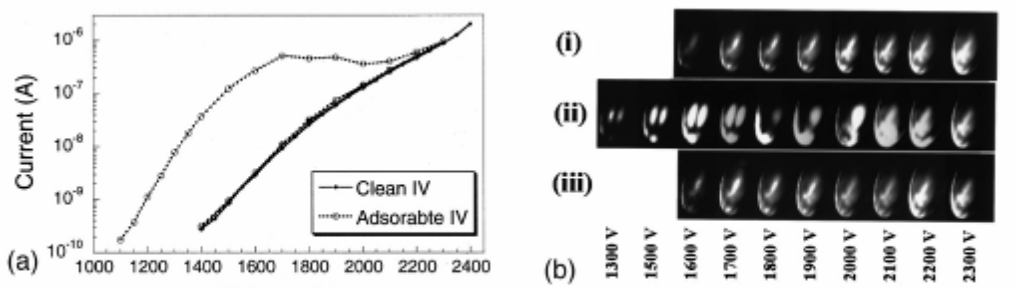

Figure 6.13: (a) Current–voltage characteristic of a single nanotube with and without adsorbates (b) The field emission pattern of a clean nanotube is stable over the voltage sweep (i) but the pattern of the same nanotube with an adsorbate changes during the current–voltage sweep concurrent with the onset of current saturation (ii). At 2300 V, the effects of the adsorbates disappear, resulting in a clean nanotube field emission pattern. During the downward I–V sweep, the images (iii) match the clean nanotube shown in (i). *Figure from Ref. [Dea00].*

To further test the hypothesis that adsorbates lead to the behavior reported in Figure 6.13, the current was measured as a function of time for stepwise increases and decreases in the applied voltage. As shown in Figure 6.14, when the applied voltage is increased to above the current saturation in Figure 6.13, the current decreases between the steps, an indication that adsorbates are being re-arranged or removed at the nanotube tip. For the downward sweep, the current is found to increase between steps as adsorbates re-attach and re-occupy configurations with higher tunneling rates.

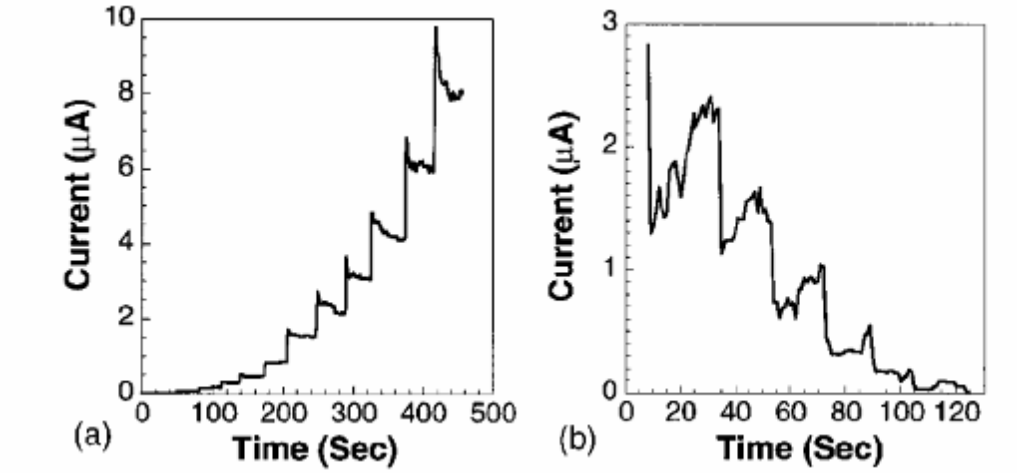

Figure 6.14: Time-dependence of field-emission current when the applied voltage is changed in a stepwise fashion. In (a), the applied voltage is increased to above that of the saturation in Figure 6.13, and the current decreases as adsorbates re-arrange and desorb from the nanotube tip. In (b), the applied voltage is decreased, and the current increases between steps as adsorbates re-attach to the nanotube tip. *Figure from Ref. [Dea00].*

6.3 Nanotube Arrays

We have so far discussed field emission from a single nanotube or a single bundle. Applications in display devices will however involve carbon nanotube films or arrays because of the need for field emission over large areas. To be competitive with conventional field emitters, the nanotube films should exhibit uniformity with an areal density larger than 10^6 emitters/cm^2 and current densities of 80 μA/cm^2 [Nil00]. However, in exploring high-density nanotube arrays for field emission, it is observed that the emission is not better for high densities, but in fact is maximized at intermediate densities [Nil00]. To probe the origin of this behavior, a scanning field emission technique with a Pt-Ir anode with a tip radius of 2-5 μm was employed to obtain a spatially resolved field emission image from nanotube films of different densities patterned as a grid. Figure 6.15 shows the printed pattern and higher magnification scanning electron microscope images (left) of patterned nanotube films of low, medium and high areal densities, and the associated scanning field emission scans. At low densities, the emission is inhomogeneous and comes mostly from localized regions in the film, presumably where there are nanotube with larger length-to-diameter ratios (and thus enhanced β factors). At high densities, some of the patterned lines are visible, but a clear pattern is not obtained. The sample with medium density provides the best image of the emission pattern: the lines, crosslines, and dashes can be seen. The improved emission properties at intermediate densities originate from a combination of two factors. At low densities the pattern has very few efficient emitters while the enhancement factor in the high density pattern is reduced because of electrostatic screening between neighboring nanotubes. To verify this last hypothesis, simulations of the equipotential lines in an array of carbon nanotubes of different densities have been performed [Nil00]. The calculations indicate that the field penetration diminishes as nanotubes are packed more densely and this affects both β and the total emitted current. Figure 6.15 shows the field penetration in an array consisting of nanotubes of length 1 μm and radius 2 nm. Clearly the penetration is poor when the spacing between nanotubes is 0.5 μm (bottom) as opposed to 4 μm (top). The corresponding field enhancement factor decreases rapidly as the nanotube separation is decreased below 2 μm, and the simulated current density peaks at nanotube spacings of 2 μm. This maximum in the current density is a consequence of the interplay between the areal density and field amplification factor β in determining the total emitted current.

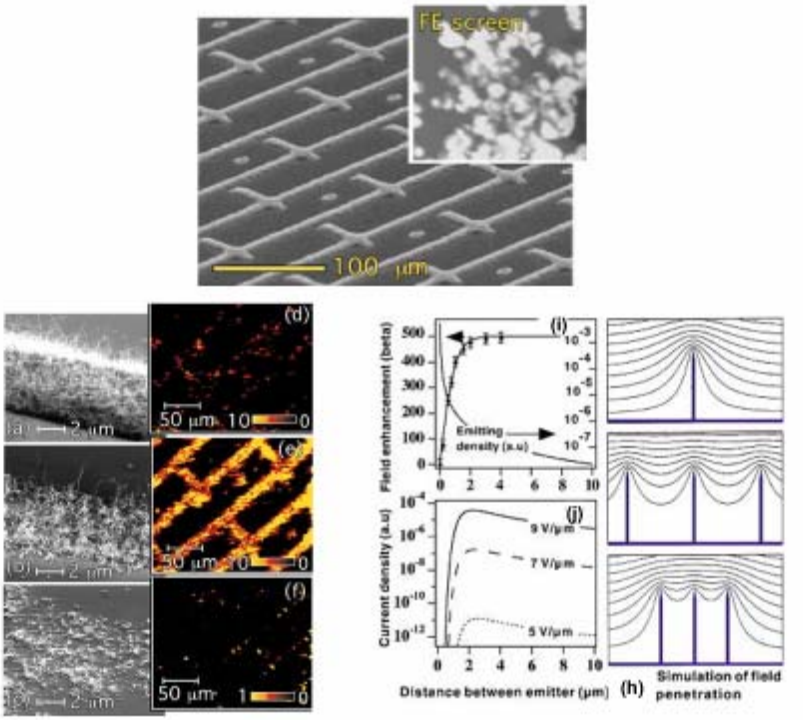

Figure 6.15: The top image shows a low magnification scanning electron microscope image of a carbon nanotube film patterned in the form of lines. Inset is the macroscopic field-emission pattern captured on a phosphor screen. The left-most panels show higher magnification scanning electron microscope images of the patterned carbon nanotube films with (a) high, (b) medium, and (c) low density, with the corresponding field emission maps of current density (d)–(f). The color scale corresponds to 0-10 μA/pixel for images (d) and (e); and to 0–1 μA/pixel in image (f). (h) Simulation of equipotential lines of the electrostatic field for tubes of 1 μm height and 2 nm radius, for distances between tubes of 4, 1, and 0.5 μm, (i) Field enhancement factor and emitting density, and (j) current density, as a function of the distance between nanotube emitters. *Figures from Ref. [Nil00].*

6.4 Failure Mechanism

Because of the high electric fields required for field emission, materials for field emission tips must be able to withstand the high temperatures generated by Joule heating and the high stress generated by the electric field. These harsh conditions can lead to degradation of the device performance, and ultimately breakdown. For carbon nanotube tips, it was originally proposed that the maximum temperature reached along the nanotube is at the tip [Vin02], implying that breakdown of the nanotube should occur in a fairly continuous fashion by shortening at the tip. However, experimental work has demonstrated that breakdown of nanotube tips during field emission occurs a few tens of nanometers away from the tip [Wei07b]. An example of such an observation is shown in Figure 6.16. There, a multiwall carbon nanotube attached to a tungsten tip is imaged using a transmission electron microscope, with several images taken in sequence as the field

emission voltage is increased. The images indicate that for this nanotube (diameter of 14 nm and length of 330 nm) the initial damage occurs about 50 nm from the tip in the form of a cleave; further increase of the applied voltage leads to further damage in this area eventually causing the nanotube end to be burned off. (It should be noted that a different breakdown mechanism, where the nanotube detaches from the tungsten tip is also observed for weaker bonds between the nanotube and the tungsten [Bon03].) Similar observations of breakdown away from the tip has been observed in other nanotube samples [Wei07b, Doy06]

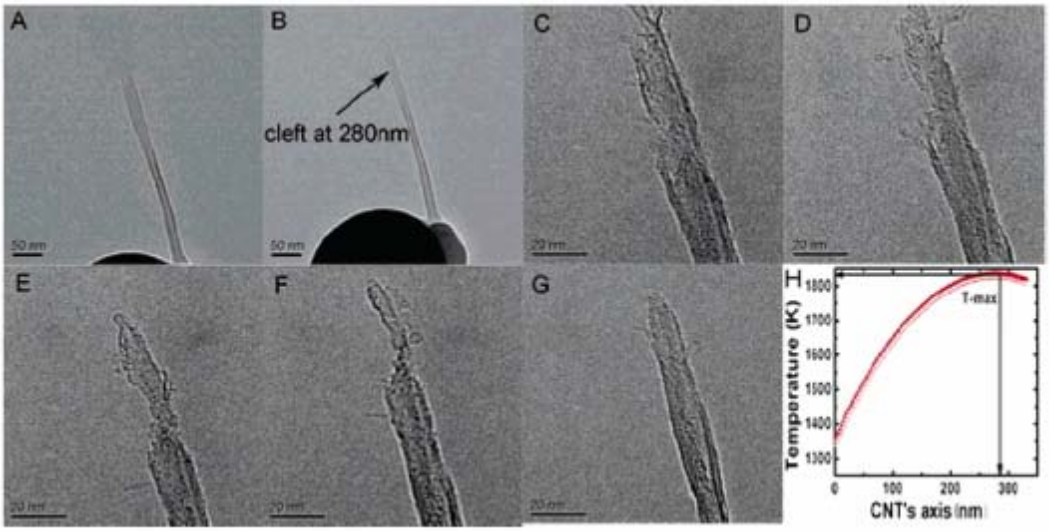

Figure 6.16: Transmission electron microscopy images of the failure process of a carbon nanotube tip during field emission (A-G) and the predicted temperature profile along the nanotube (H). *Figure from Ref. [Wei07b].*

To understand the origin of the nanotube breakdown away from the tip end, a theoretical model based on Joule heating has been proposed [Wei07b]. In this model, a nanotube of length L is attached to a tungsten tip at one end, as illustrated in Figure 6.17. The temperature profile along the nanotube is determined by the heat conduction equation

$$ms\frac{\partial T}{\partial t} = \kappa v \nabla^2 T + \frac{dQ}{dt} \tag{2.18}$$

where T is the spatially-dependent temperature, κ is the thermal conductivity, v is the sample volume, m is the mass, s is the specific heat and Q is the heat. The heat dissipated in the nanotube comes from two sources: the electrical resistance (Joule heating) and heat radiation. These can be written as

$$\begin{aligned} \frac{dQ_{elec}}{dt} &= I^2 \rho v \\ \frac{dQ_{rad}}{dt} &= -\sigma A\left(T^4 - T_0^4\right) \end{aligned} \tag{2.19}$$

where the first relation is simply Joule's law with current I and resistivity ρ, and the second equation is the Stefan-Boltzmann law for radiation, with σ the Stefan-Boltzmann constant for a body of surface area A emitting into surroundings at temperature T_0. (A note of caution: strickly speaking, Equation (6.19) is not entirely correct. In principle, Joule heating and heat radiation occur only from the surface of the nanotube, so that, for example, the Joule heating should be written as $dQ_{elec}/dt = I^2 \rho v \delta(r-R)$, and similarly for the heat radiation. The presence of the delta function is expected to influence the length scale over which the temperature distribution varies along the carbon nanotube. This is similar to the effects discussed in Chapter 4 in the context of the electrostatics of carbon nanotube *p-n* junctions. Research is currently underway to address this point in more detail. Nevertheless, the effects discussed in this section are expected to remain qualitatively correct, and the formulation in Equation (6.19) has the advantage of simplifying the solution.)

For one-dimensional heat transport in the steady-state we have

$$\pi R^2 \kappa \frac{\partial^2 T}{\partial x^2} - 2\pi R \sigma \left(T^4 - T_0^4\right) + \frac{I^2 \rho}{\pi R^2} = 0. \tag{2.20}$$

To solve this equation, an expression for the temperature dependence for the resistivity is needed, as well as boundary conditions. An empirical, nonlinear expression for the dependence of the resistivity on temperature has been proposed [Hua04] to reproduce experimental data of resistitivy at high temperatures [Pur02, Col01]:

$$\rho(T) = \rho_0 \left(1 - \alpha T + \beta T^{3/2}\right) \tag{2.21}$$

where ρ_0 is the resistivity at room temperature and α, β are fitting coefficients. The boundary conditions at the interface with the microtip and at the free end are determined as follows. At the nanotube/microtip interface, there is a temperature drop due to the thermal contact resistance equal to

$$\frac{T_0 - T(x=0)}{\lambda} = Q = -\kappa \pi R^2 \frac{\partial T}{\partial x} \tag{2.22}$$

with the parameter λ representing the quality of the thermal contact, and where we have assumed that the microtip is at temperature T_0. This provides an expression for the temperature at the microtip end of the nanotube

$$T(x=0) = \lambda \pi R^2 \kappa \left.\frac{\partial T}{\partial x}\right|_{x=0} + T_0. \tag{2.23}$$

The interesting physics that differentiates carbon nanotubes from conventional field emitters arises at the free end. When an electron is emitted at the free end, it carries energy, and this effectively cools the tip. In conventional metals, cooling due to field-emission is typically much smaller than radiative cooling—in carbon nanotubes however, the field emission current density is very large while the surface area for radiative cooling is small, making field-emission cooling a dominant factor. To take into account this

effect, the heat loss due to the energy carried away by the field-emitted electrons is assumed to occur at the free end of the nanotube, assuming that each electron carries energy $(3/2)kT_L$ with T_L the temperature at $x = L$. From Fourier's heat conduction relation one obtains the boundary condition

$$\left.\frac{\partial T}{\partial x}\right|_{x=L} = -\sigma\kappa^{-1}\left(T_L^4 - T_0^4\right) - \frac{3}{2}\kappa^{-1}\frac{kT_L I}{e\pi R^2}. \tag{2.24}$$

With the boundary conditions provided by Equations 6.23 and 6.24, and the relationship between the resistivity and temperature provided by Equation 6.21, the differential equation for the temperature distribution (6.20) can be solved to obtain the spatial dependence of the temperature in the carbon nanotube. Figure 6.17 shows the calculated temperature distribution for parameters extracted from experiment [Wei07]. In the absence of the tip cooling effect (black triangles) the maximum temperature is reached at the tip of the nanotube. In contrast, in the presence of tip cooling, the maximum temperature is reached significantly away from the tip, with a much reduced maximum temperature. Since it is expected that failure will occur at the point of maximum temperature, this model predicts that carbon nanotube failure during field emission will occur some distance away from the tip end. In fact, application of the above model to the nanotube of Figure 6.16 predicts a maximum temperature at a point 50 nm from the tip end, in very good agreement with the experiment.

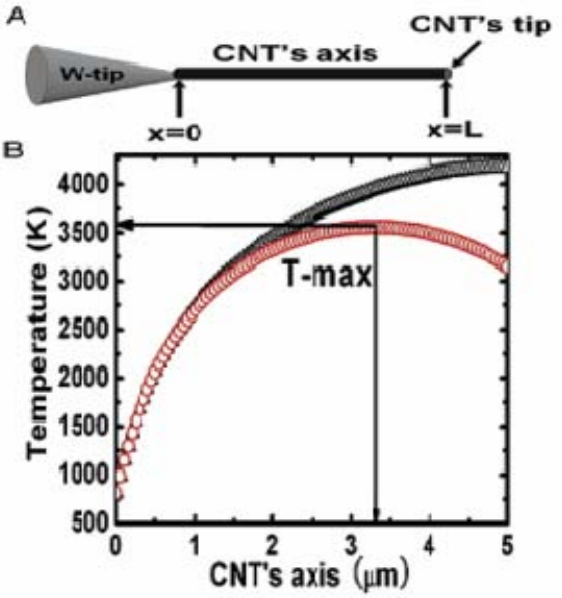

Figure 6.17: (A) Schematic of the field emission tip, consisting of a carbon nanotube of length L attached to a tungsten tip. (B) Calculated temperature distribution along the carbon nanotube in the presence (red) and absence (black) of heat loss due to electron emission. *Figure from [Wei07b].*

Finally two points should be noted: First, the maximum temperature that is reached along the length of the nanotube decreases with a decrease of the nanotube length, with or without the tip cooling effect. This serves as a mechanism to stabilize the nanotube and

prevent additional failure. Second, Joule heating is but one mechanism that can lead to breakdown during field emission (we have already mentioned breakdown at the nanotube/microtip interface above). In addition to Joule heating, there is a large electrostatic force on the carbon atoms during field emission which can lead to large axial and radial stresses. The total breakdown mechanism is probably due to a combination of heating and field effects.

6.5 Devices

Field Emission Displays: Displays using the superior field emission properties of carbon nanotubes have been demonstrated by a number of research groups. Compared to the emissive displays based on microfabricated tips [Tal01], carbon nanotube cathodes offer the potential for improved performance (i.e. lower drive voltage, longer lifetime, and a reduced fabrication cost). Figure 6.18 shows a multicolor display demonstrated in reference [Cho99b]. The display consists of carbon nanotube tips on a patterned metal substrate, with the carbon nanotube bundles firmly attached to the metal electrode. The nanotubes are mixed with an organic nitrocellulose to form a paste and then squeezed through a wire mesh to force alignment of nanotubes perpendicular to the metal. The density of nanotubes obtained is about $5x10^6$ to 10^7 cm^{-2}, which is about one hundred times larger than the density of microtips in conventional spindt type field emission displays. Since the initial work of reference [Cho99b], nanotube-based displays have become an important area of research and development, and Samsung demonstrated a 38-inch color television in 2003.

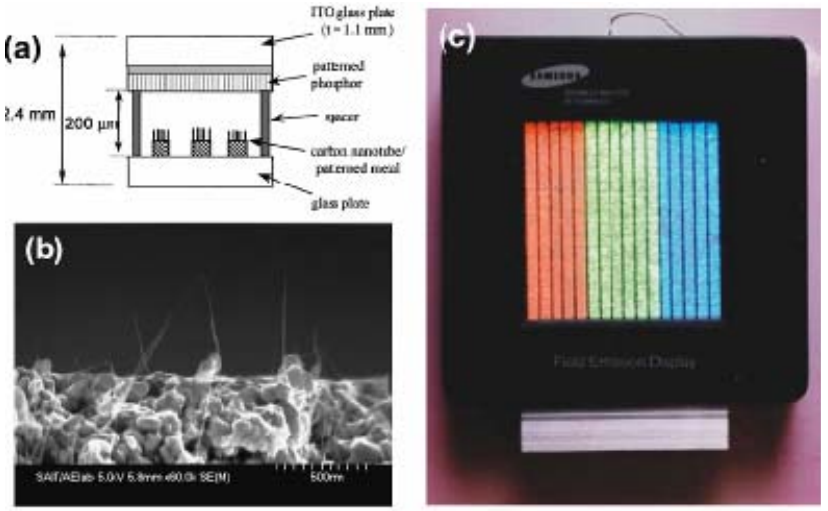

Figure 6.18: (a) Picture representing the setup of a field emission display. Carbon nanotubes are deposited on a patterned metal substrate. Field emitted electrons hit the phosphor screen and cause light emission in a color that depends on the chemical compound on the phosphor screen. (b) Scanning electron microscope image of nanotube bundles projecting from the metal electrode. (c) A sealed carbon nanotube field emission display emitting light in three different colors. The dimension of the display is 4.5 inches. *Figure from Ref. [Cho99b].*

X-ray tubes & spectrometers: X-ray sources have many medical and industrial applications, in addition to their use as a spectroscopy tool in materials science. In conventional x-rays tubes, thermionically emitted electrons from a heated metal filament are accelerated and then strike a metal target, which releases x-rays. The high power consumption and small response times of thermionic sources makes x-ray generation using cold field emission attractive. Also, the high temperatures of thermionic sources place limitations on both the size and lifetime of x-ray tubes. Ultra-sharp metal field emission tips obtained by micromachining have suffered from problems related to mechanical and thermal stability due to arcing and cation sputtering [Sug01, Yue02]. Like in field emission displays, the advantage of cold field emission from carbon nanotubes offers a potential to build x-ray tubes that are smaller, portable, use low power, and have long lifetime. Carbon nanotubes overcome many problems associated with metal field emission tips because they are mechanically strong and can withstand higher temperatures.

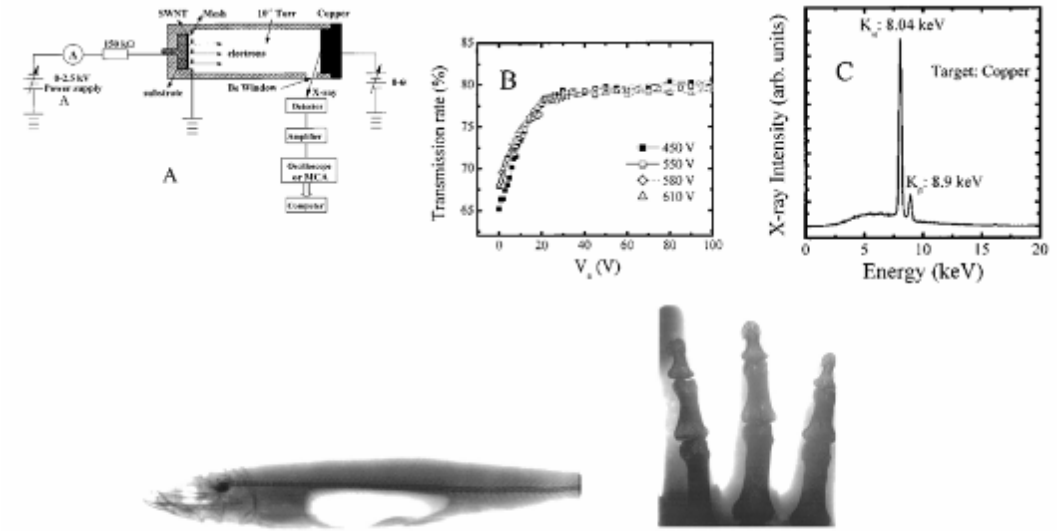

Figure 6.19: (A) Schematic of an x-ray tube using a triode with carbon nanotube field emission. The gate electrode is a metal mesh placed between 50 and 200 μm from the nanotube film. X-rays are produced when the accelerated electron beam from the nanotube film impinges on a copper target. (B) Fraction of field emission current detected at the anode. (C) Energy distribution of the x-ray produced from the copper target, showing the K_α and K_β lines. Bottom: X-ray images of a fish and a human hand. *Figures from Ref. [Yue02].*

Many applications of x-ray tubes require currents in the range of 50 – 500 mA/cm^2. Obtaining such high and stable current densities over macroscopic areas using nanotubes has been challenging. However, recently, current densities as large as 1 A/cm^2 have been obtained [Yue02, Sar04], though their stability over long periods of operation has not been determined. Carbon nanotube x-ray tubes have been demonstrated to be capable of imaging circuit boards [Sug01] and human hands [Yue02]. The basic working principles of these x-ray imaging devices is fairly simple: a high-energy electron beam strikes a metal target, releasing x-rays. A schematic of such a device using a film of carbon nanotubes as the electron emission source is shown in Figure 6.19. There, a metal mesh is

positioned at a distance of tens to hundreds of microns from the carbon nanotube film, which consists mostly of bundles of single wall carbon nanotubes. A high voltage applied between the metal mesh and the nanotube film causes electron emission; these electrons impinge on a copper target. When the incoming electrons have sufficiently high energy, they can knock out core electrons in the metal atoms, and as higher energy electrons transition to this lower energy level, photons are emitted with energy typically in the keV range. To realize an x-ray source from cold cathode field emission in a triode geometry, it is important that most of the field emission current passes through the metal mesh and impinges on the metal target, so as to prevent excessive heating of the mesh electrode. For the carbon nanotube device in Figure 6.19, optimization of the mesh density and separation from the nanotube film leads to a high transmission of 80% through the mesh. At an acceleration voltage of 14 kV, these transmistted electrons generate x-ray lines of 8.04 keV and 8.9 keV, corresponding to the K_α and K_β lines of copper.

More recently, a compact multibeam nanotube x-ray source capable of three-dimensional imaging (two dimensional frames at various angles) has been demonstrated [Zha05]. The operation voltage of these x-ray tubes is in the 15 – 50 kV range, which is comparable to conventional sources. Another recent demonstration has been x-ray tubes for spectroscopy applications using a carbon nanotube field emission source (Figure 6.20). This x-ray tube uses only 1.5 – 3 W, and operates on batteries. Using such a small x-ray tube, a field deployable x-ray spectrometer called CheMin that weighs only 15 kg has been built [Sar04]. CheMin has been chosen to be a science instrument to fly in the Mars '09 Science Laboratory mission, and will perform mineralogy experiments on the surface of Mars (Figure 6.20).

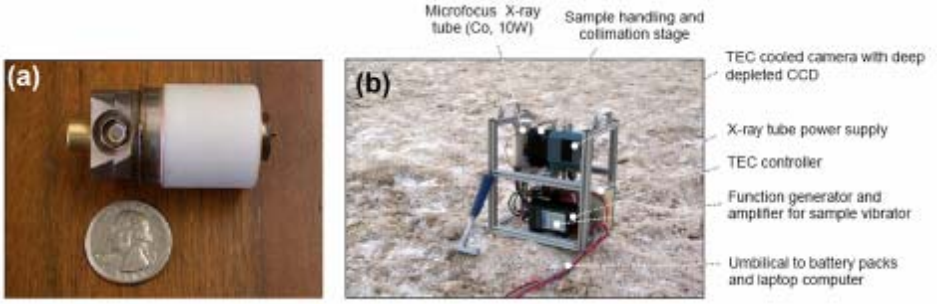

Figure 6.20: (a) A miniature field emission x-ray tube made of a 2 mm diameter multiwall nanotube cathode. *Figure from Ref. [Sar04]* (b) CheMin, a portable x-ray spectrometer, with a geologist's hammer for scale. *Figure from Ref. [Sar05].*

Field-emission lamps:

Conversion of energy into lighting is a significant portion of the world's energy consumption, with up to 8% of the total energy and 22% of electricity converted into lighting in the U.S. [Phi06]. Currently, 42% of the lighting energy in the U.S. is used by incandescent light bulbs, which are extremely inefficient since most of the energy is wasted as heat. Alternatives to this centuries-old technology are actively sought, and field-emission lamps are possible candidates—a sketch of a possible device is shown in Figure 6.21. There, a cylindrical cathode covered with field-emission tips isotropically emits electrons that are captured by a phosphor layer on the cylindrical anode. For this

kind of uniform, non-directed illumination, isotropic field emission from a cylindrical surface is needed. Difficulties in depositing or fabricating a high density of field-emitters on a cylindrical surface have prevented the development of such an approach using conventional materials. Carbon nanotubes may provide a solution to this problem because it is possible to cover a metallic cylindrical rod homogeneously with a catalyst and grow nanotubes catalytically. Such an approach has been demonstrated using a Fe-Al-Cr alloy on which a liquid Fe catalyst is applied, and the nanotubes are grown by the catalytic decomposition of acetylene [Bon01]. This results in a metallic cylindrical rod of 1 mm diameter and 7 cm in length homogeneously covered with a tangle of multi-wall carbon nanotubes. The field emission lamp is fabricated by positioning the cylindrical rod in the center of a cylindrical aluminum anode of 21 mm radius and 5 cm length, in a vacuum chamber. Field emission is induced by applying a large voltage between the cylindrical rod and the cylindrical anode, giving a very large current density of 1 mA/cm^2 at a voltage of 1.1 kV. This large current density is due to the large electrical field at the cathode in the cylindrical geometry [Bon01]. Indeed, in the cylindrical geometry, the electric field at the surface of the cathode is

$$E_{cyl} = -\frac{V}{R_C \ln\left(R_A / R_C\right)} \tag{2.25}$$

where R_C is the radius of the cathode and R_A is the radius of the anode. This can be compared with the expression $E_{planar} = -V/d$ for two planar electrodes separated by distance *d*. The ratio $E_{cyl}/E_{planar} \approx \left(R_A/R_C\right)/\ln\left(R_A/R_C\right)$ can be quite large: for the field emission lamp of reference [Bon01] the ratio is about 11, and when combined with the exponential dependence of field-emission, can lead to much larger emitted currents for similar physical dimensions.

Figure 6.21 shows a field emission lamp fabricated using a cylindrical cathode covered with carbon nanotubes. The anode is a glass tube coated with ITO and a phosphor layer on the inside surface. The luminescence of this lamp is 10 000 cd/m^2, comparable to a commercial fluorescent tube. (The power consumption is however much higher, mostly due to the inefficient phosphor utilized in this prototype device). The carbon nanotube field emission lamp has many advantages over conventional fluorescent lamps: it is better for the environment because it contains no mercury, it starts up instantly, and the light intensity can be easily varied by controlling the field emission voltage. Futher technological progress in this area has recently allowed the fabrication of a fully-sealed prototype device (see Figure 6.21 and [Jon04b]).

Figure 6.21: Left: Sketch of a field emission lamp using a cylindrical cathode covered with carbon nanotubes. Electrons emitted from the cathode strike a phosphor layer on the anode to cause illumination. Middle and right: prototypes of luminescent tubes using cylindrical carbon nanotube cathodes. The device on the right is fully sealed. *Figures from [Bon01] and [Jon04b].*

In addition to cylindrical illumination, field-emission lamps also have potential for large area flat illumination. Triode structures seem to be the most promising for such applications and attempts have been made at fabricating such structures with carbon nanotube field emitters [Cho07]. The biggest challenge in large area applications is that the suspended metal mesh used for the gate vibrates under the large applied electric fields causing non-uniformity in the electron emission current due to variations in the distance between the gate and the cathode, arcing, and increased leakage current. To address these issues it has been proposed to use a metal mesh patterned with trenches and holes and bonded to the cathode plate [Cho07], in addition to being coated with SiO_2 to reduce the leakage current. In this design (Figure 6.22), trenches in a stainless steel metal mesh of 150 micron thickness and 64 cm^2 area are created, and the mesh is perforated with 170 micron diameter holes using a wet etching process. A layer of SiO_2 is deposited on the mesh using plasma-enhanced chemical vapor deposition. The cathode consists of a soda-lime glass on which a thin layer of Ag is deposited; a paste of multiwall carbon nanotubes is printed onto the Ag layer in the form of dots with 40 micron diameter and 6-8 micron thickness. Finally, the metal mesh is bonded to the cathode using glue, and the phosphor-coated ITO anode is combined with the cathode and the metal mesh using 3 mm spacers.

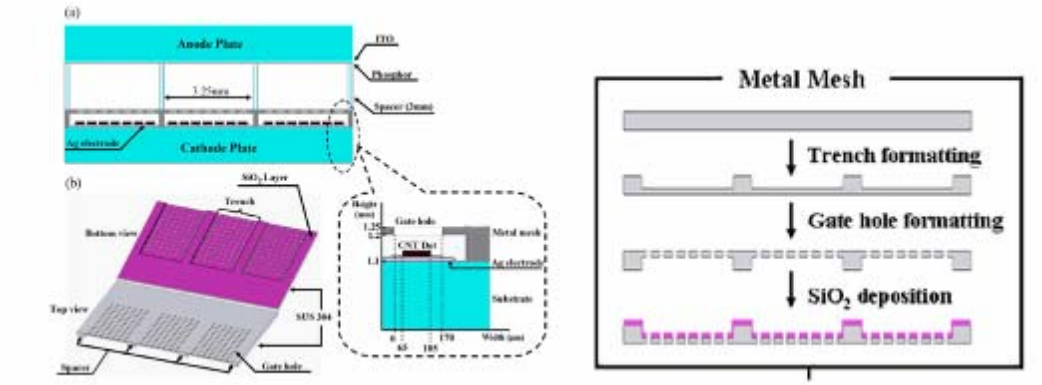

Figure 6.22: (a) Sketch of a triode field emission lamp for large area illumination using carbon nanotube emitters. (b) Sketch of the metal mesh and fabrication process (right). *Figures from Ref. [Cho07].*

Figure 6.23 shows the anode current as a function of the gate voltage, for an anode voltage of 4.5 kV. The anode current shows a turn-on behavior with a turn-on gate voltage of 160 V; comparing the anode and gate currents, it is seen that the anode current is about 8 times larger than the gate leakage current. When impacting the phosphor-coated anode, the large field-emitted current leads to a uniform screen illumination as shown in Figure 6.23. For comparison, a similar device was fabricated, but without bonding the metal mesh to the cathode and showed a much less uniform emission pattern due to the increased vibrations of the metal mesh. The brightness of the uniformly illuminating device is found to be 6000 cd/m^2. In addition to improving the uniformity of

the emission, the bonded metal mesh also reduces the arcing and allows for stable operation of the device even under the very large anode voltages applied.

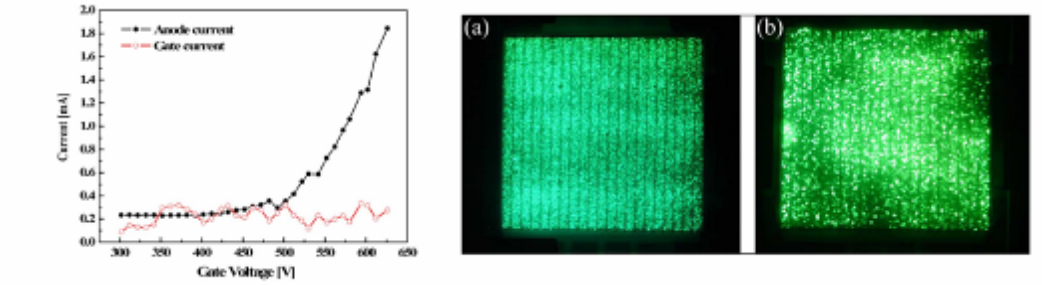

Figure 6.23: Left: Field emission and gate leakage currents as a function of the gate voltage in a triode fied emission lamp. (a) and (b): Illumination of the green phosphor at the anode using the field-emitted current. The image labeled (a) has a bonded metal mesh as the gate, while that in image labeled (b) has an undonded metal mesh. *Figures from Ref. [Cho07].*